Supporting Information

Flexible-rigid covalent nano-template of micron porous silicon towards ultra-robust Li-ion battery

Baoping Liu,[a] HanJiang Li,[a] Wen Luo,*[a] Xiaofeng Zhang,*[b] Zhongyun Liu,[c] Pengfei Yin[d] and Rui Zhang *[d]

[a] School of Materials and Energy, Guangdong University of Technology, Guangzhou 510006, China

[b] Institute of New Materials, Guangdong Academy of Sciences, Guangzhou 510650, P. R. China

[d] School of Chemical and Biomolecular Engineering, Georgia Institute of Technology, Atlanta, Georgia 30332, United States

[d] Institute of New-Energy Materials, School of Materials Science and Engineering, Tianjin University, Tianjin, 300072, China

* Corresponding author: Wen Luo (wenluo@gdut.edu.cn) or Xiaofang Zhang (zxf200808@126.com) or Rui Zhang (ruiz@tju.edu.cn)

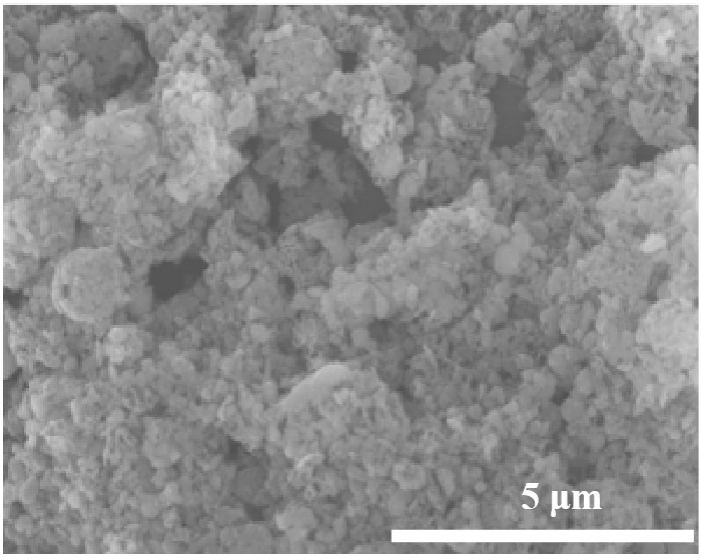

Figure S1. SEM image of MPSi by directly acid etching

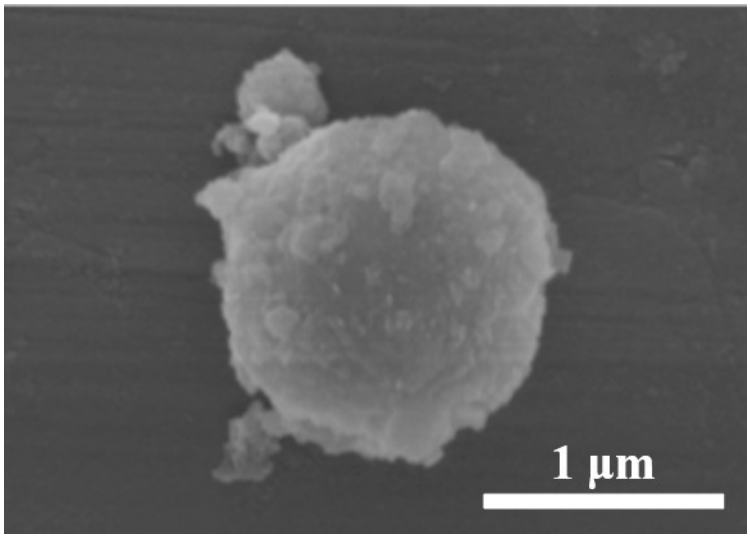

Figure S2. SEM image of AlSi@RTiO_2

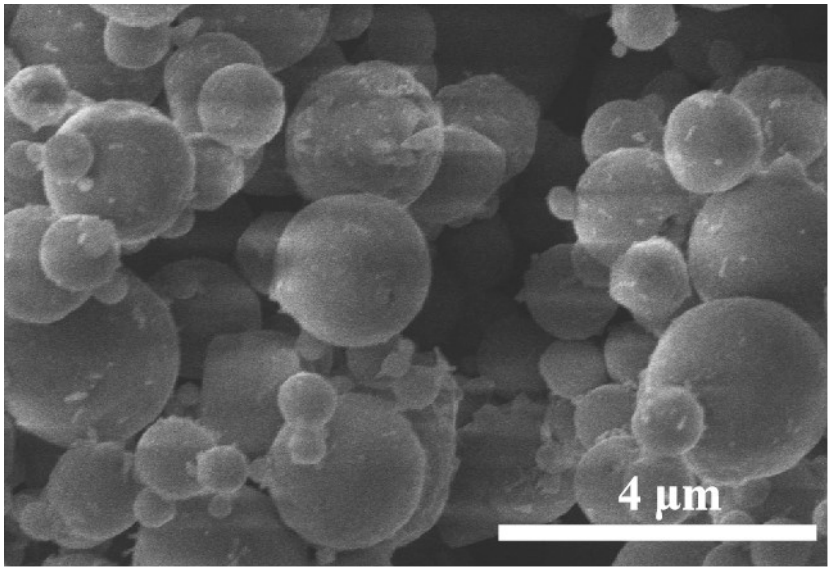

Figure S3. SEM image of AlSi alloy

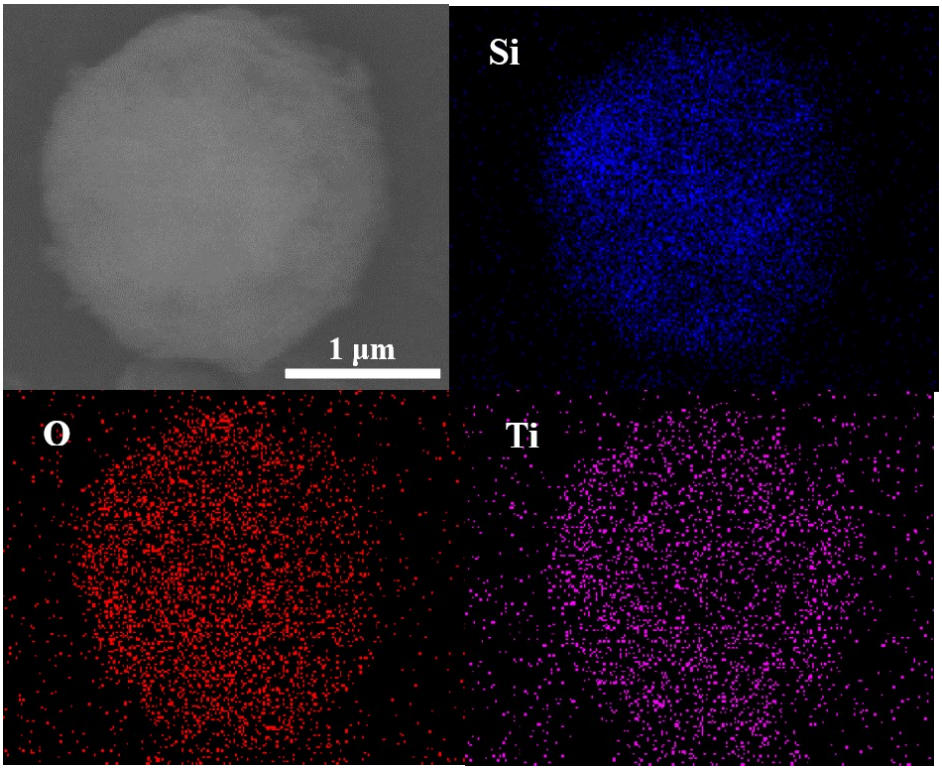

Figure S4. EDS image of the MPSi@RTiO_2

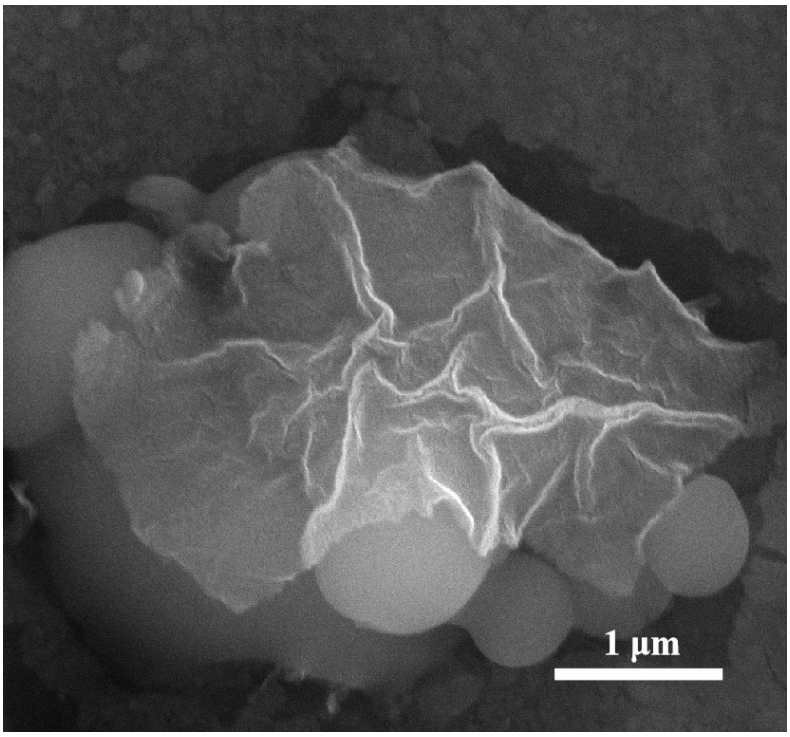

Figure S5. SEM image of molten salt and $FG_{N,P}$

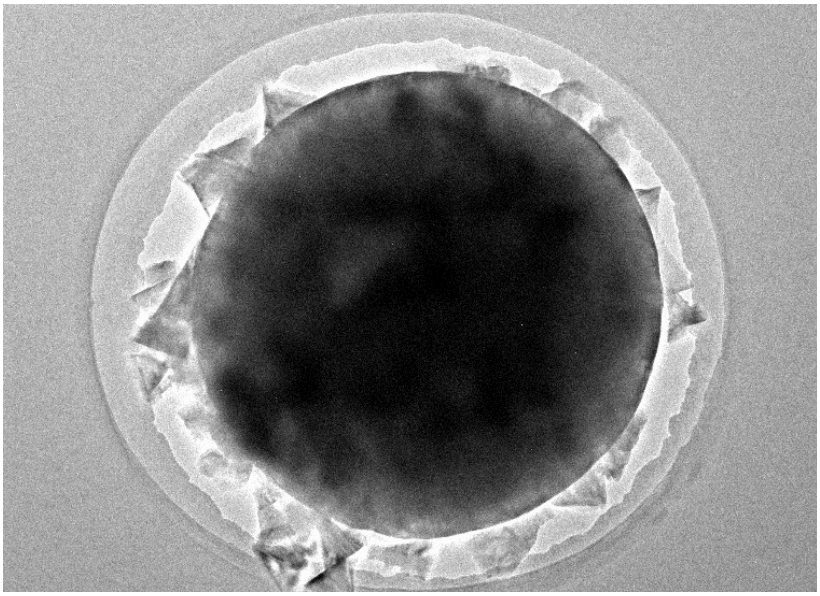

Figure S6. TEM image of AlSi alloy

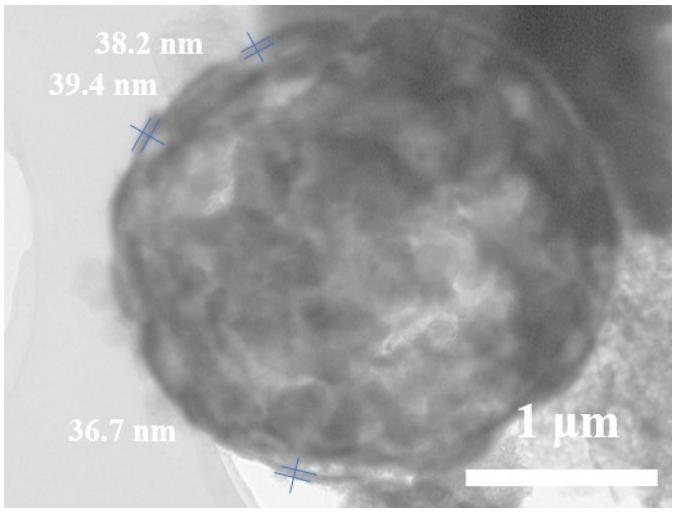

Figure S7. TEM image of MPSi@RTiO$_2$.

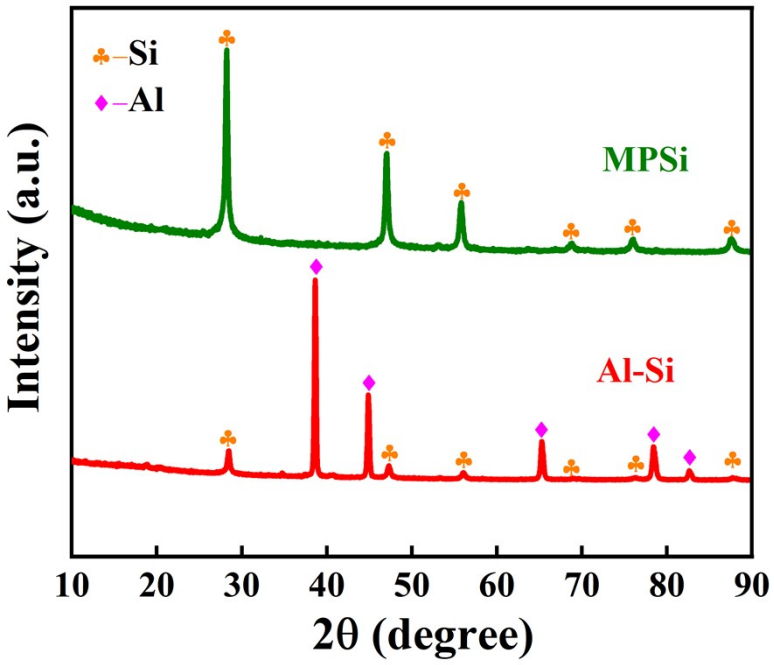

Figure S8. XRD image of Al-Si and MPSi

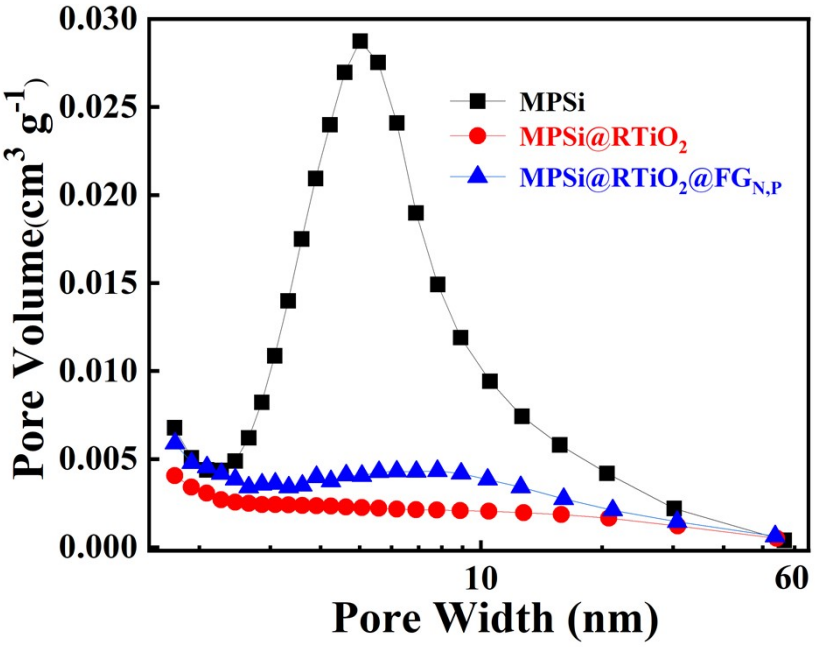

Figure S9. Pore size distributions.

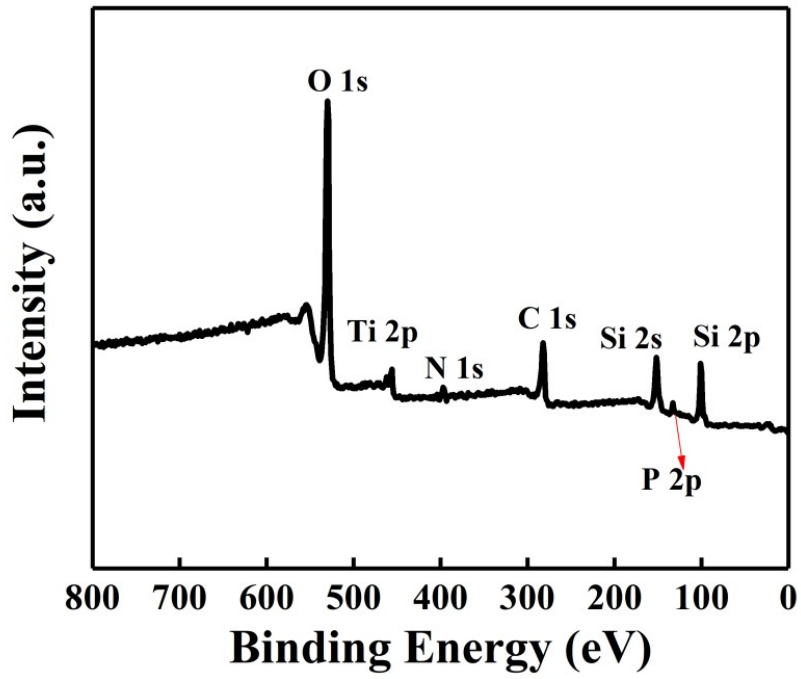

Figure S10. The XPS total spectrum of MPSi@RTiO$_2$@FG$_{N,P.}$

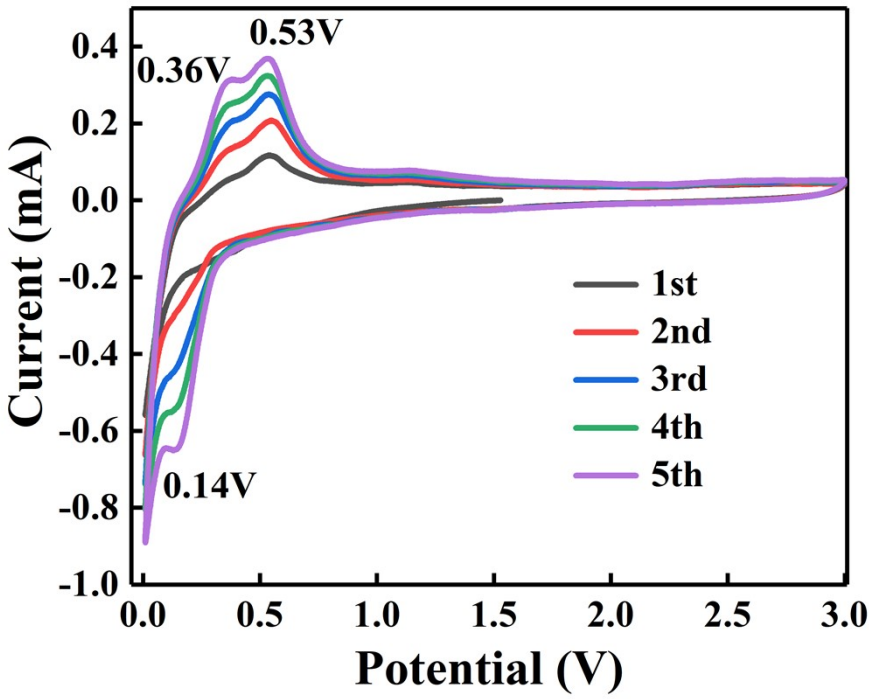

Figure S11. CV curves of MPSi at the first five cycles

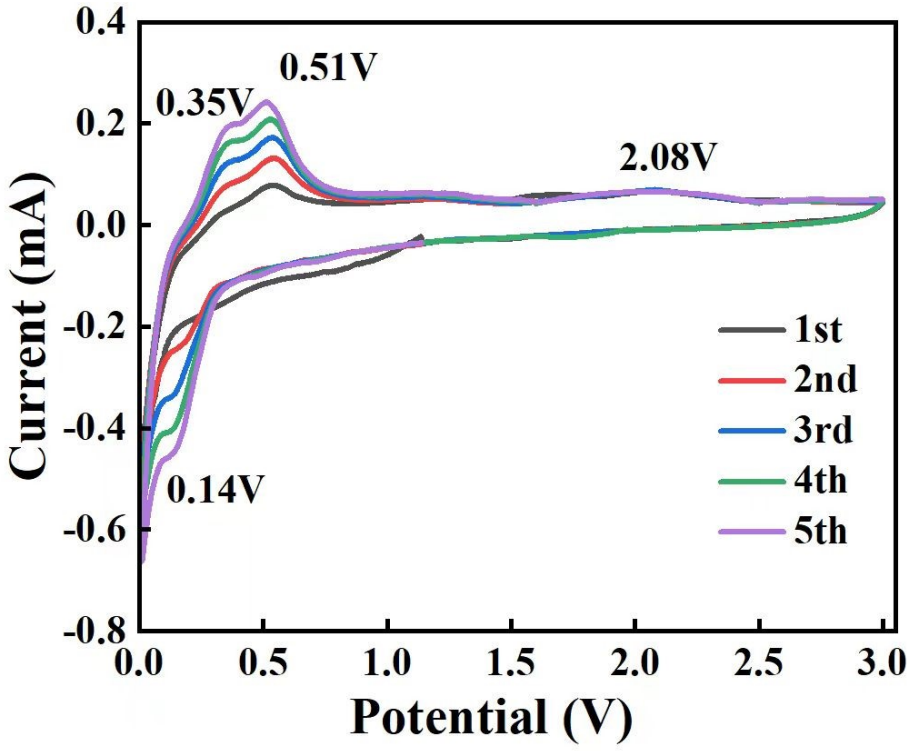

Figure S12. CV curves of MPSi@RTiO_2 at the first five cycles

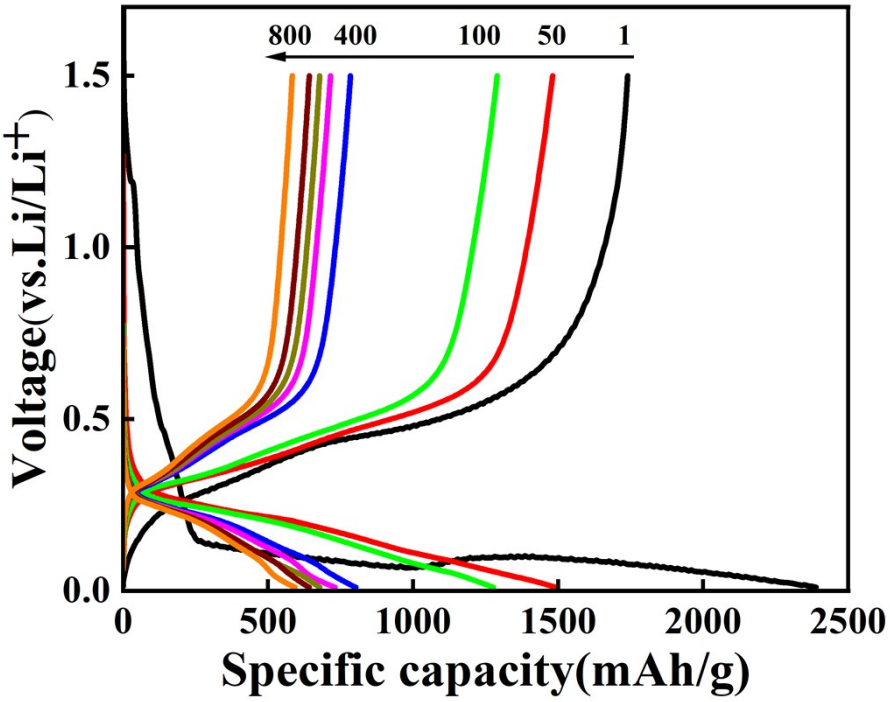

Figure S13. Charge/discharge voltage profiles of MPSi@RTiO$_2$

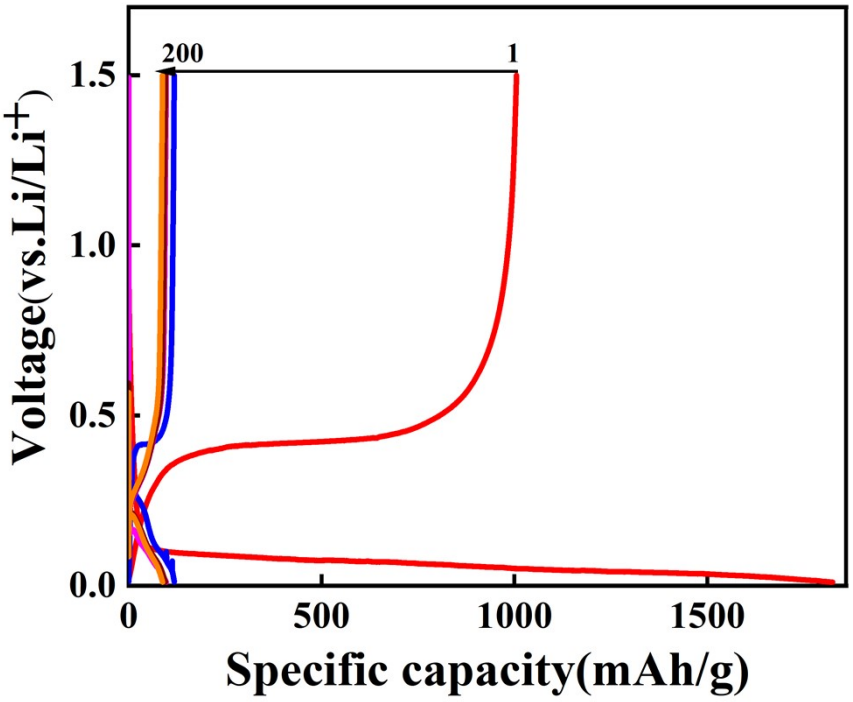

Figure S14. Charge/discharge voltage profiles of MPSi

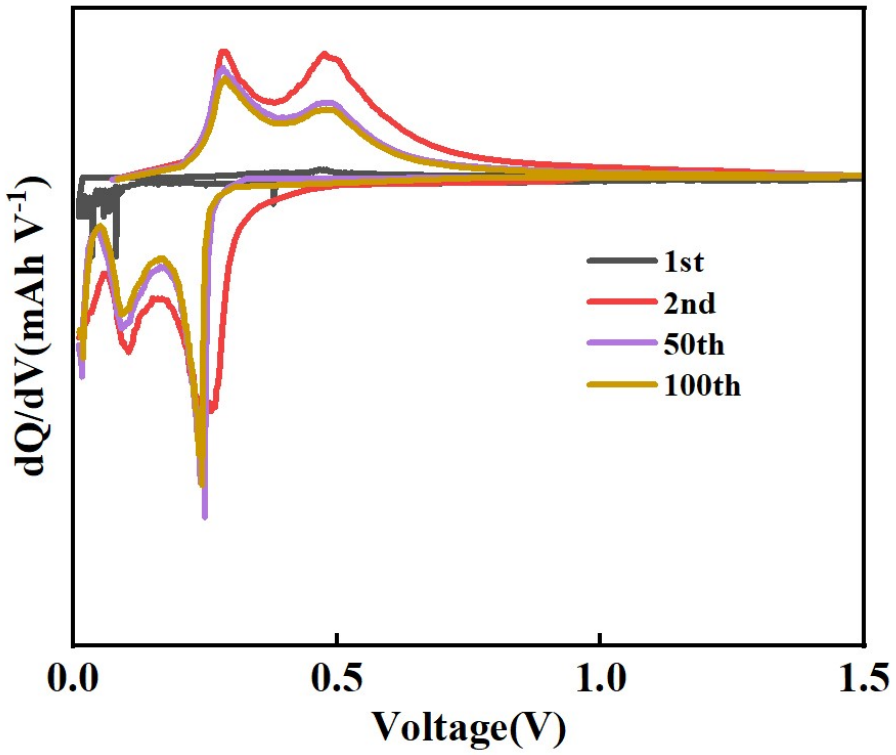

Figure S15. Differential capacity (dQ/dV) profiles of MPSi@RTiO$_2$@FG$_{N,P}$ anode.

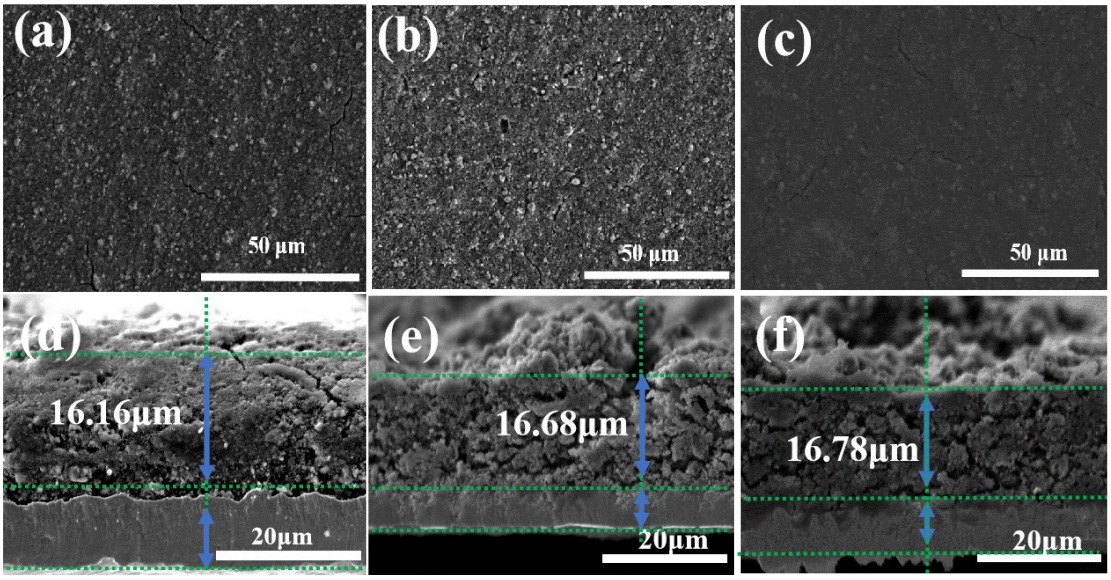

Figure S16. SEM image before electrode cycle (a, d) MPSi, (b,e,) MPSi@RTiO$_2$ (c,f) MPSi@RTiO$_2$@FG$_{N,P}$

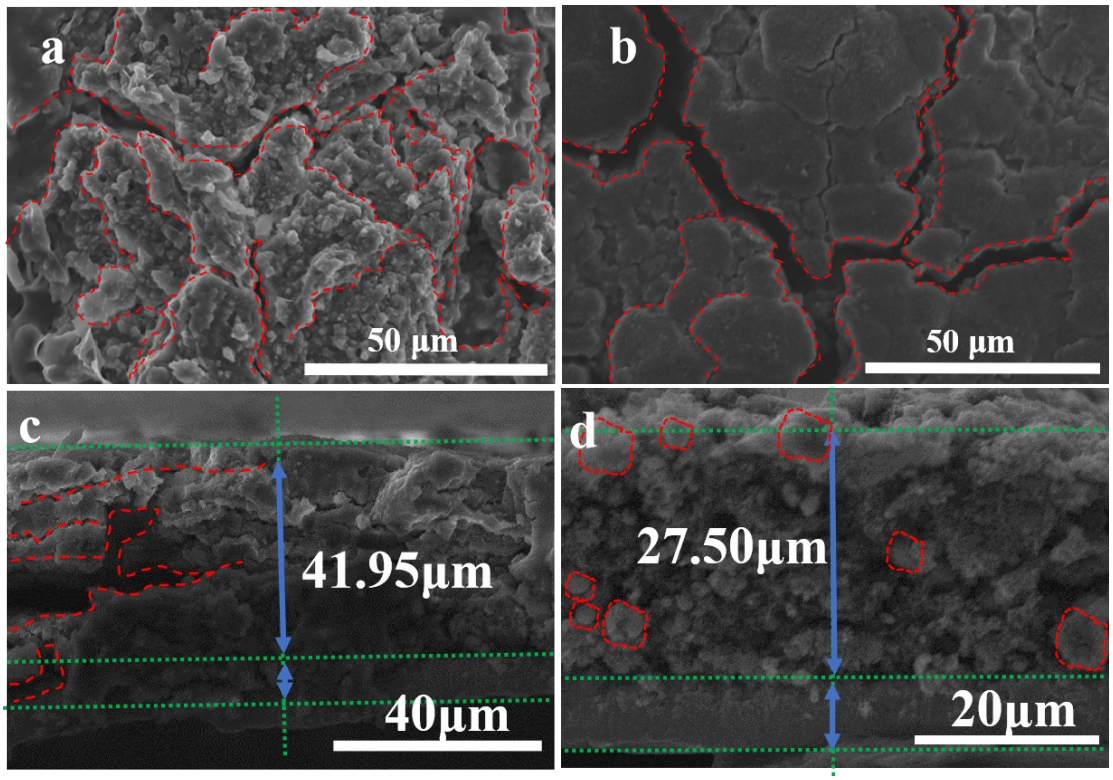

Figure S17.SEM images of the microscopic morphological changes of electrodes in the long-cycling process at 1000mA g^{-1}. (a, c) MPSi electrode after 200 cycles and (b, d) MPSi@RTiO$_2$ electrode after 600 cycles.

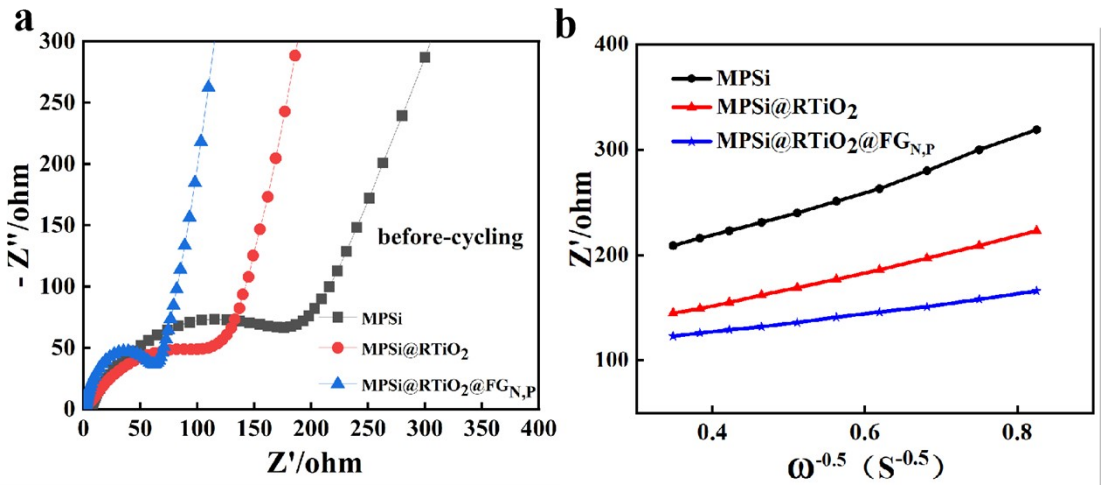

Figure S18. (a) electrochemical impedance spectroscopy, and (b) relationship between Z 'and $\omega^{-1/2}$ at lower angular frequencies

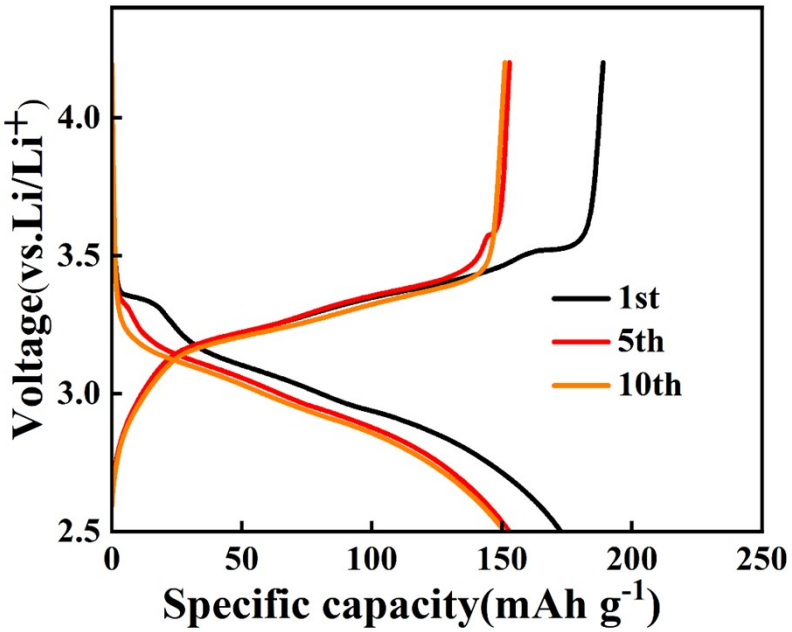

Figure S19. Charge/discharge voltage profiles of MPSi@RTiO$_2$@FG$_{N,P}$//LFP full cell

Table S1. The detailed data of ICP test

Sample	element	mass (g)	volume (mL)	dilution ratio	instrument reading (mg/L)	concentration	unit
MPSi@RTiO$_2$@FG$_{N,P}$	Si	0.0597	50	50	17.5445	741409.1604	mg/kg
MPSi@RTiO$_2$@FG$_{N,P}$	Ti	0.0597	50	50	2.6765	113104.4624	mg/kg
MPSi@RTiO$_2$@FG$_{N,P}$	N	0.0597	50	50	0.0498	2106.1456	mg/kg
MPSi@RTiO$_2$@FG$_{N,P}$	P	0.0597	50	50	0.0213	902.4497	mg/kg

Table S2. Comparison of synthesis strategies and electrochemical properties of micron silicon-based anode materials for lithium ion batteries

anodes	Loading (mg/cm^2)	Initial CE (%)	capacity (mA h g^{-1}) after assigned cycles at a current density (A g^{-1})	refs
MPSi@RTiO$_2$@FG$_{N,P}$	**2.9**	**81.2**	**1014/800/1**	**this work**
PSi@CNS	0.5	74.6	1272/500/1	12
SiMP/SHP/CB	0.5	80	900/500/1	15
PAA-P(HEA-co-DMA) binder with SiMP	1	89.3	2245/255/1	17
mSi@OG@RGO	1	78	1750/160/2	19
PSi/SCNT-SRGO	0.6	81.1	1008/600/1	23
p-Si@C	0.6	58	868/300/1	28
SiO_x/C-CVD	1.5	67.4	972/500/0.5	32
P-Si/rGO	1.5	80.96	1258/300/1	34
EB	0.65	87.9	2300/200/1	35